Influence of Hot-Dip Galvanization on the Fatigue Performance of High-Strength Bolted Connections

A. Milone[1*], P. Foti[2], L.M. Viespoli[3], D. Wan[4], F. Mutignani[5], R. Landolfo[1], F. Berto[6]

[1]Department of Structures for Engineering and Architecture (DiST), University of Naples "Federico II", Via Forno Vecchio 36, 80134, Naples (Italy)
[2]Department of Mechanical Engineering (MTP), Norwegian University of Science and Technology, Richard Birkelands vei 2B, 7034, Trondheim (Norway)
[3]Department of Materials and Nanotechnology, SINTEF Industry, 7456, Trondheim, Norway
[4]Advance Research Institute of Multidisciplinary Science (ARIMS), Beijing Institute of Technology, Beijing, Beijing 100081 (China)
[5]CEN/TC250/WG09 Expert, Viale F. Petrarca 96, 35028 Piove di Sacco (Padua), Italy
[6]Department of Chemical, Material and Environmental Engineering (DICMA), Sapienza University of Rome, via Eudossiana 18, 00184, Rome (Italy)
*Correspondence

Abstract

In the present work, the influence of hot-dip galvanization (HDG) on the fatigue behaviour of high-strength bolted details is investigated through a set of 15 constant-amplitude tests. Cyclic behaviour of coated specimens is hence compared against results for unprotected samples drawn from literature, i.e., both with reference to neutral and aggressive exposure conditions. Namely, while behaviour of coated samples is moderately inferior as respect to uncoated ones in dry air (–6% in terms of characteristic fatigue strength, probability of failure P_F = 5%, confidence interval CI = 75%), their performance still complies with European normative requirements for double covered joints, and galvanization proves to be highly effective when corrosion is likely to occur (with a characteristic strength increase of [+12%; +52%]). Finally, fractography analyses on both uncoated and coated specimens were performed, suggesting that hydrogen embrittlement may play a role in reducing fatigue strength of coated joints, that is, especially within the high-cycle fatigue regime.

Keywords: *Fatigue behaviour; Hot-dip galvanizing (HDG); Bolted connections; Structural steel*

1 Introduction

Steel structures such as railway bridges and offshore constructions are often subjected to the combined action of *i*) repeated loads and *ii*) detrimental exogenous agents (i.e., moisture, saline water, etc…) owing to their peculiar destination of use [1]. Therefore, proper protective measures are usually adopted to prevent or retard material degradation, which might otherwise induce sudden corrosion fatigue (CF) collapse in presence of significant cyclic actions [2].

Two major strategies can be pursued for corrosion protection (CP), i.e. *active* and *passive* protection, which can be further combined into hybrid systems when appropriate [3].

On one hand, active CP involves the use of direct current to manipulate the electric potential of metallic surfaces to be protected and thus slow down corrosive processes. Although being highly efficient, this technique is often costly and affected by power shutdowns, as it requires a constant electricity supply [3, 4].

On the other hand, passive CP benefits of either *i*) the physical barrier offered by non-conductive materials (e.g., bitumen, polymeric resins) or *ii*) the higher reactivity of certain metals (e.g., Zn or Al alloys) acting as *sacrificial anodes* on which corrosive processes are redirected. In both cases, passive protection is usually adopted in form of surficial coatings [3-4].

Passive CP systems can represent a highly competitive option for new bridges and offshore structures, i.e., owing to their affordability and ease of implementation. Among the wide range of available surface treatments, hot-dip galvanization (HDG) stands as one of the most common options to improve the performance of steel components from a durability perspective, namely due to its adaptability to a large set of steel grades and structural details [6-11]. HDG involves the immersion of metallic elements in a bath of melted zinc (≈ 450° C) and their subsequent cooling in a quench tank, resulting in a thin sequence of bonded layers of Zn–Fe alloys acting as sacrificial anodes [12].

Nevertheless, as highlighted by various researchers, HDG may potentially impair the fatigue performance of structural steel details, as the surface alteration leads to multiple, potential crack initiation spots [13-16]. Namely, while Bergengren et al. [17] related the reduction of fatigue strength to the zinc layer thickness t_{Zn}, other researchers did not find a clear correlation between fatigue properties and t_{Zn} [18-19]. Within this framework, Vogt et al. [20] estimated a threshold value for t_{Zn} (≈ 60 μm) below which no influence on the fatigue performance is expected for unnotched mild steel components.

However, it should be remarked that considerations reported in Berto et al. [6, 14], Ferraz & Rossi [13], Rademacher et al. [15], Ungermann et al. [16] and Bergengren et al. [17] imply assuming pristine structural details as a reference condition, while possible benefits of HDG in terms of extension of the service life should be more properly assessed as respect to corroded details.

To this end, it is worth mentioning the contributions of Adaasoriya et al. [21-22], which investigated the reduction of fatigue strength in worn steel smooth components. Accordingly, *i*) the constant-amplitude fatigue limit (CAFL) $\Delta\sigma_{D,corr.}$ of corroded elements can reduce to 0.55 ÷ 0.75 times the relevant CAFL in pristine conditions $\Delta\sigma_D$, *ii*) the inverse slope of Wöhler curves *m* can increase up to 1.4 times as respect to reference values and *iii*) no endurance limit $\Delta\sigma_{L,corr.}$ should be assumed for corroded elements. Analogous conclusions were drawn by Jiang et al. [23] and Jikal et al. [24] with regard to pitted high strength steel (HSS) wires. For the relevant case of high-strength bolts and bolted details, complying remarks were pointed out by Zampieri et al. [25], Lachowiz et al. [26], Li et al. [27] and Jiang et al. [28], which highlighted the influence of increased fretting wear on the fatigue life of corroded specimens, i.e., due to premature crack initiation at worn contact surfaces [25-28].

Therefore, the convenience of HDG for steel structures located in aggressive environments is still a question far from being solved up to present time [13]. To this end, while more contributions can be found in scientific literature with respect to plain members and welded details [13, 14-20, 29], only few results are available regarding bolted connections [6].

Assessing the fatigue performance of galvanized bolted connections is a crucial task, as bolting is one of the most popular assembling techniques, i.e., due to its intrinsic cost-effectiveness, practicality and reliability [30]. Nevertheless, while bolted details are often adopted in steel constructions placed in aggressive environments [2], there is still some scepticism in protecting them with HDG when significant cyclic loads are expected [13]. For instance, the Italian Railway Network (RFI) does not provide any indication about HDG for railway bridges details, i.e., due to concerns about the fatigue performance reduction [31, 32].

If one considers the long service life required for such constructions (up to 100 ÷ 120 years), the resulting increase of maintenance costs proves to be considerable as respect to an initial HDG treatment.

Therefore, the main aims of this paper are *i*) to widen the small bulk of fatigue data related to galvanized high-strength bolted details, i.e. allowing to more clearly investigate the influence of HDG on the cyclic performance

of such connections, *ii*) to assess the impact of HDG with reference to a common structural detail which is still not covered by current European fatigue provisions and *iii*) to compare the cyclic behaviour of galvanized bolted details with respect to pristine (unprotected) and corroded conditions, with the latter being of major practical interest when dealing with aggressive exposure conditions. For this purpose, a set of 15 constant-amplitude fatigue tests on galvanized bolted assemblies made with L profiles has been carried out. In order to provide a benchmark in terms of fatigue performance, three specimens were not galvanized (see Section 2.1 for further details).

In order to ensure a robust statistical assessment, the bulk of fatigue data has been widened by also considering *i*) the few literature outcomes for galvanized bolted joints (Berto et al. [6]) and *ii*) the Eurocode background fatigue data for uncoated, preloaded bolted joints as recollected by Maljaars & Euler [33]. Results are hence compared with EN1993:1-9 [34] and DNVGL-RP-C203 [35] recommendations for pristine and corroded details. Namely, as no indications are reported in EN1993:1-9 [34] as respect to damaged connections, normative Wöhler curves are corrected according to suggestions from Adasooriya et al. [21-22].

The present work is hence divided in three parts. In the first Section, main features of bolted specimens are presented. Therefore, in the second part, fatigue results are presented, discussed and compared against provisions in force. Finally, in the last Section, further insights on the effect of HDG in terms of fatigue behaviour are provided through fractography analysis.

2 Materials and Methods

2.1 Main features of tested specimens

Main geometrical features of tested specimens are depicted in Figure 1. The adopted configuration resembles real details employed in steel railway bridges (Unsworth [36], Denton [37]). Each specimen consists of two 45 × 45 × 4 mm L profiles and two 300 × 80 × 12 mm plates made of European S235 JR steel grade (characteristic yield stress f_y = 235 N/mm^2). Elements were connected by means of 5 × 2 pre-loaded HV M12 high-strength bolts (Class 10.9, each one equipped with plain gaskets), with 14 mm bolt holes being realized through drilling. Bolt pre-loading was applied by means of a calibrated wrench up to a final torque of 91 Nm (i.e., corresponding to an estimated preload of [48 kN; 75 kN] = [0.57 $F_{u,b}$; 0.88 $F_{u,b}$] according to simplified normative formulations [38] – with $F_{u,b}$ being the ultimate tensile resistance of the bolt). Notably, assembled specimens comply with EN1993:1-8 [38] requirements in terms of limit distances for connections in shear.

In compliance with Berto et al. [6], profiles and plates were hot-dip galvanized by immersion in a molten Zn bath for a total time of 14 minutes before assembling. The resulting zinc layer had a thickness $t_{Zn} \approx 400$ μm. Fasteners were hot-dip zinc coated as well according to ISO 10684 provisions [39].

In order to remove the outer layer of pure Zn, which is overly soft and malleable, connections surfaces were treated by means of a *sweep blasting* process (i.e., a light sandblasting treatment) according to ISO 8503 indications [40].

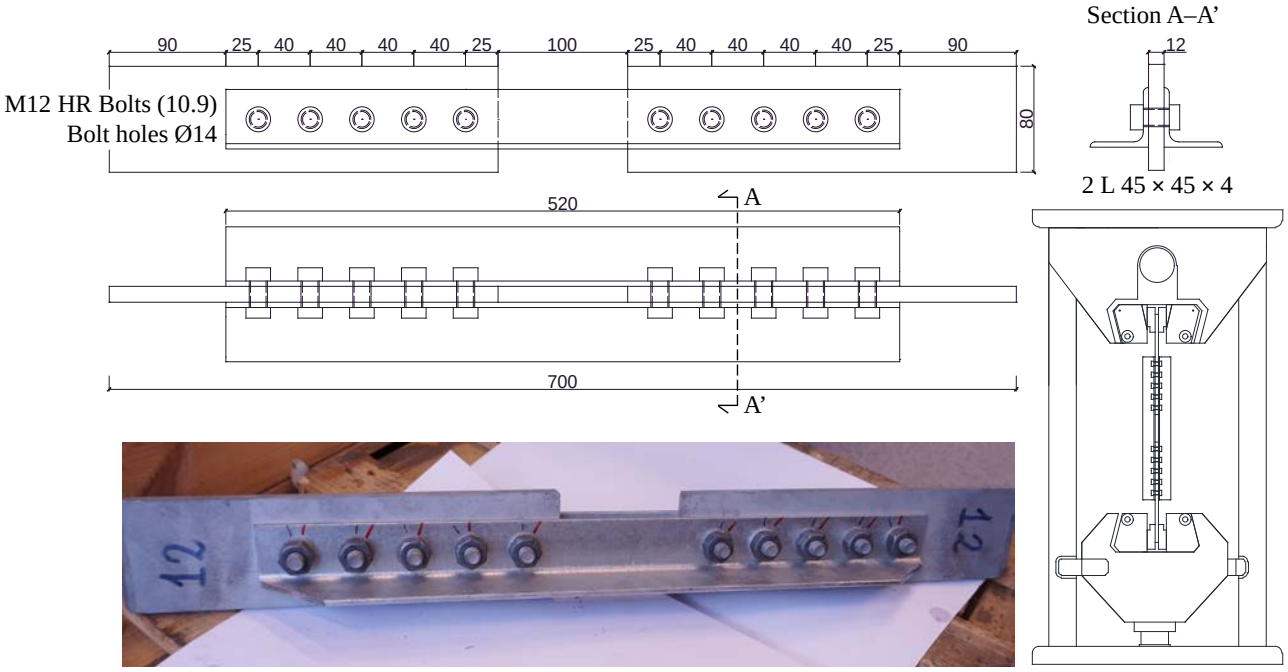

Figure 1 – Test setup and main geometrical features of coated & blasted high-strength bolted specimens (measures in mm).

As stated earlier, in order to *i*) provide a preliminary benchmark for the fatigue performance of uncoated specimens and *ii*) to check whether the behaviour of such samples is in line with normative and literature remarks for comparable bolted details, three (out of fifteen) specimens having identical geometry were not galvanized or sandblasted before testing. This ensures that possible differences in the fatigue behavior has to be demanded to the coating process whose effect on the fatigue properties represents the aim of the present work.

2.2 Constant-amplitude fatigue tests

Constant-amplitude fatigue tests were performed using the *Instron 8854 Axial-Torsion System* Universal Machine, which features a servo-hydraulic dynamic test system and a combined axial/torsional actuator having a maximum capacity of ±250 kN/ ±2000 Nm. In order to mainly focus on the influence of *i*) the detail configuration and *ii*) the galvanization process, a constant load ratio R = 0 was assumed for all tests, i.e., preliminarily disregarding the impact of mean-stress effect [33], and the same load frequency f_{test} = 10 Hz was always selected. In order to avoid overly long tests, a runout threshold for cycles at failure $N_{max} = 2 \cdot 10^6$ was assumed.

A proper labelling has been introduced to uniquely identify each test. For instance, the first two letters refer to the specimens' surface treatment conditions – i.e., NC for not coated ones and ZS for galvanized and sweep blasted ones – and they are followed by two numbers in reference to the order of performed tests.

Fatigue test results are summarized in Figure 2 and Table 1 in terms of nominal stress range $\Delta\sigma$ against the number of cycles at failure N_f (Wöhler or S-N curves).

Table 1 – Fatigue tests results (load ratio R = 0, f_{test} = 10 Hz were assumed for all specimens). Stress ranges evaluated in the gross cross-section of the most stressed elements, that is, the two L profiles, according to EN1993:1-9 [34].

Label [-]	Treatment [-]	Load Range ΔF [kN]	Nominal Stress Range $\Delta\sigma$ [N/mm^2]	Number of Cycles at Failure N_f [-]	Fracture Spot [-]
NC01	Uncoated	180	257.7	76826	L - Hole
NC02		240	343.5	7996	L - Hole
NC03		140	200.4	567161	L - Hole

ZS01	Galvanized and Sweep Blasted	100	143.1	2000000+	Runout
ZS02		160	229.0	150112	L - Hole
ZS03		140	200.4	211622	L - Gross
ZS04		180	257.7	74987	L - Hole
ZS05		120	171.8	751640	L - Gross
ZS06		240	343.5	15874	L - Hole
ZS07		200	286.3	42205	L - Hole
ZS08		200	286.3	58316	L - Gross
ZS09		240	343.5	14001	L - Hole
ZS10		160	229.0	110227	L - Hole
ZS11		120	171.8	715469	Plate - Hole
ZS12		100	143.1	2000000+	Runout

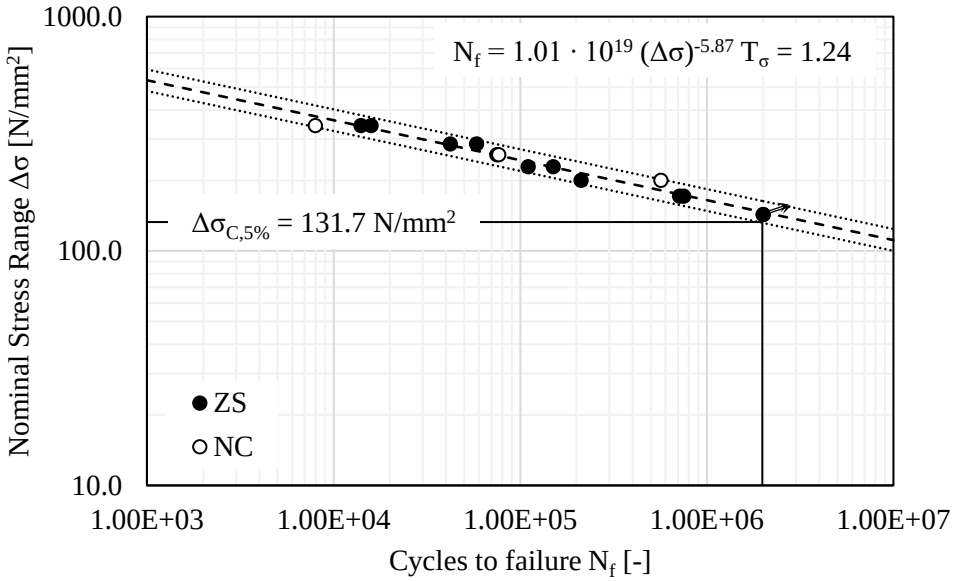

Figure 2 – Fatigue test results.

For the sake of clarity, tests resulting in a runout are highlighted with an arrow or in grey, respectively. Scatter bands referred to the entire set of tests (NC + ZS) are depicted as well. According to EN1993:1-9 [34] provisions for pre-loaded bolted connections, and consistently with literature results on similar uncoated assemblies [33], stress ranges are referred to the gross cross-section of the most stressed elements, that is, the two L profiles ($A_{2L,gross} = 2 \times 349.3 = 698.6$ mm^2).

Statistical assessment of results is reported in Table 2 in terms of *i*) equivalent detail classes (DC) $\Delta\sigma_{C,PF}$ for different values of failure probability P_F, *ii*) inverse logarithmic slope *m* of the Wöhler curves, i.e., supposed independent of P_S [41] and *iii*) scatter ratio (SR) $T_\sigma = \Delta\sigma_{C,95}/\Delta\sigma_{C,5}$. According to EN1993:1-9 [34] and DNVGL-RP-C203 [35] recommendations, DCs were estimated for $N_f = N_C = 2 \cdot 10^6$, P_F = 5% – 50% – 95%

were assumed so as to provide characteristic and mean values of fatigue strength and a 75% confidence interval was considered.

For the sake of comparison, data analysis has been performed both with reference to the lone set of galvanized and blasted specimens (ZS) and to the entire ensemble of fatigue tests (NC + ZS). Owing to the limited number of samples (n = 3), assessment for sole NC specimens has been omitted.

It is worth remarking that, although being commonly used in bridge design [36-37], tested details are not explicitly addressed by normative provisions [34-35]. Thus, in order to assess their fatigue performance within the framework of European codes, a reference DC was selected based on structural similarities; that is, in light of *i*) the nominal absence of out-of-plane bending due to longitudinal symmetry and *ii*) the prevalence of friction mechanism (i.e., due to gaskets-profiles and profiles-plates contact) for transferring shear loads, tested samples were assimilated to preloaded double covered joints (detail category "112" [34] and "C1" [35], respectively – $\Delta\sigma_C$ = 112 N/mm^2 in both cases). Notably, as the assumed DC is the highest among all categories for bolted details [34-35], cautionary comparisons are hence presented in the following.

On one hand, it can be noticed how both NC and ZS specimens can be preliminarily ascribed to a same, narrow scatter band (T_σ = 1.24). Notably, the characteristic value of fatigue strength $\Delta\sigma_{C,5,NC+ZS}$ = 131.7 N/mm^2 is higher than the recommended DCs for uncoated specimens according to both EN1993:1-9 [34] and DNVGL-RP-C203 [35] ($\Delta\sigma_{C,5}/\Delta\sigma_C$ = 1.18). To this end, it is worth noting that EN1993:1-9 would recommend to select the immediately lower DC (100 N/mm^2, reduction of fatigue strength of –11%) for a galvanized double covered joint. As for the resulting slope of the Wöhler curve, the log-regression line is also flatter as respect to normative provisions (m = 5.87 > 3 [34-35]).

Table 2 – Statistical assessment of fatigue results.

Specimens [-]	Upper DC $\Delta\sigma_{C,95}$ [N/mm^2]	Mean DC $\Delta\sigma_{C,50}$ [N/mm^2]	Characteristic DC $\Delta\sigma_{C,5}$ [N/mm^2]	Inv. Slope m [-]	SR T_σ [-]
ZS	150.4	139.4	129.2	5.37	1.16
NC + ZS	163.1	146.5	131.7	5.87	1.24

On the other hand, if the lone ZS specimens are accounted for (T_σ = 1.16), only a slightly lower value of $\Delta\sigma_{C,5,ZS}$ = 129.2 N/mm^2 is achieved (–1.9% as respect to $\Delta\sigma_{C,5,NC+ZS}$), with the relevant S-N curve being steeper

(m = 5.37). Nevertheless, fatigue strength for $N_f = N_C$ still meets EN1993:1-9 [34] and DNVGL-RP-C203 [35] safety requirements.

As a matter of fact, the main difference in terms of fatigue behavior among NC and ZS specimens is represented by observed fracture spots (Figure 3). Indeed, while for tested NC specimens, cracks were detected in correspondence of the net cross-section of L profiles (Figure 3a), i.e., in line with EN1993:1-9 [34] and DNVGL-RP-C203 [35] predictions, ZS specimens exhibited either *i*) net-area failure of Ls (6/12 samples, see Figure 3b), *ii*) gross-area failure of Ls (3/12 samples, see Figure 3c) or even *iii*) gross-area failure of the plate in a single case (ZS11, see Figure 3d).

These outcomes, which cannot be explained within the framework of a nominal stress approach, clearly descend from the surficial alteration induced by HDG [6-20], which creates new potential cracking spots originating from the interface layer between Zn and Fe. Further insights about such phenomenon are provided in Section 3.2, where fractography analysis of ZS specimens is presented and discussed.

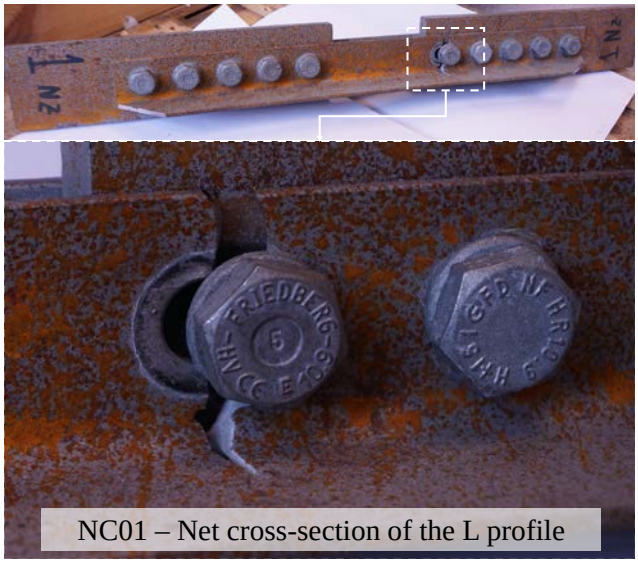

a)

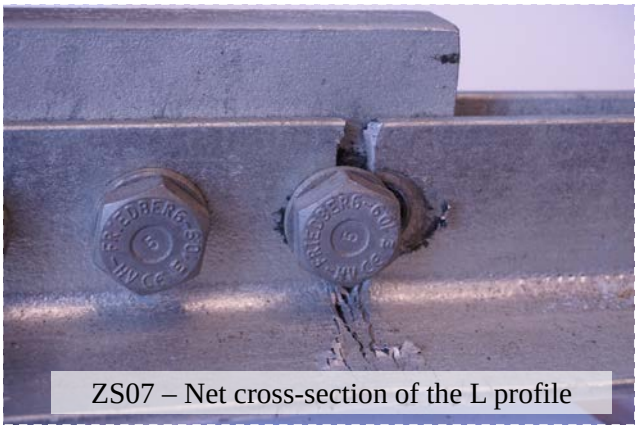

b)

c)

d)

Figure 3 – Typical fracture spots for tested a) NC, b-c-d) ZS specimens.

Nevertheless, it is worth remarking that *i*) ZS samples still failed due to net-area cracking of L profiles in 50% of the cases and *ii*) test results related to other fracture spots could be ascribed to the same scatter band with negligible dispersion ($T_{\sigma,ZS}$ = 1.16, see Table 2).

Although complying with literature remarks [6, 41], the above considerations should be intended as preliminary owing to the limited number of specimens. Therefore, in the next Section, a review of literature results on both uncoated and coated specimens characterized by the same nominal DC ($\Delta\sigma_C$ = 112 N/mm^2) is presented. Retrieved data are hence used to compare the fatigue performance of NC, ZS and corroded bolted details on a more robust basis.

2.3 Literature results

In order to widen the bulk of fatigue data related to both uncoated and coated high-strength bolted specimens, additional literature sources [6, 33] have been considered, i.e., concerning details characterized by the same category of tested connections (i.e., 112/C1 [34-35]). Berto et al. [6] investigated the fatigue performance of both uncoated and coated & blasted symmetric butt-shear bolted specimens (i.e., made of four 10 mm thick S355 plates connected by 3 × 2 M12 10.9 pre-loaded bolts). A total of 11 + 17 constant-amplitude fatigue tests (R = 0) were performed on NC and ZS specimens having identical geometry, respectively.

Maljaars & Euler [33] re-assessed the fatigue behaviour of 288 uncoated, preloaded splices with double covered plates (DC 112/C1 [30-31]) drawn from 8 literature sources [42-49], i.e., in order to provide a

background for the upcoming version of Eurocode 3 (prEN1993:1-9-2020 [50]). In order to ensure consistent comparisons against reported tests, fatigue results referred to *i*) non failed specimens (runouts), *ii*) snug-tightened joints and *iii*) bearing-type connections were excluded from analyses, i.e., resulting in a total of 244 valid test data.

In compliance with the labelling introduced in the previous Sections, test results from Berto et al. [6] and Maljaars & Euler [33] are hence identified as B-NC/B-ZS and ME-NC, respectively.

Literature results are summarized in Figures 4-5 and Table 3 in terms of Wöhler curves and statistical assessment of experimental outcomes ($\Delta\sigma_{C,PF}$, *m*, SR). For the sake of comparison, results of experimental tests illustrated in Section 2.2 are reported as well.

It is worth remarking that fatigue results reported in Maljaars & Euler [33] originally referred to multiple stress ratios $R = \sigma_{MIN}/\sigma_{MAX} = 0.0 \div 0.5$. In order to account for the influence of mean-stress effect on fatigue life [51], stress ranges were corrected to a reference zero-to-tension condition ($R_{ref} = 0.0$) according to the modified Morrow criterion as follows (Equation 1 [33]):

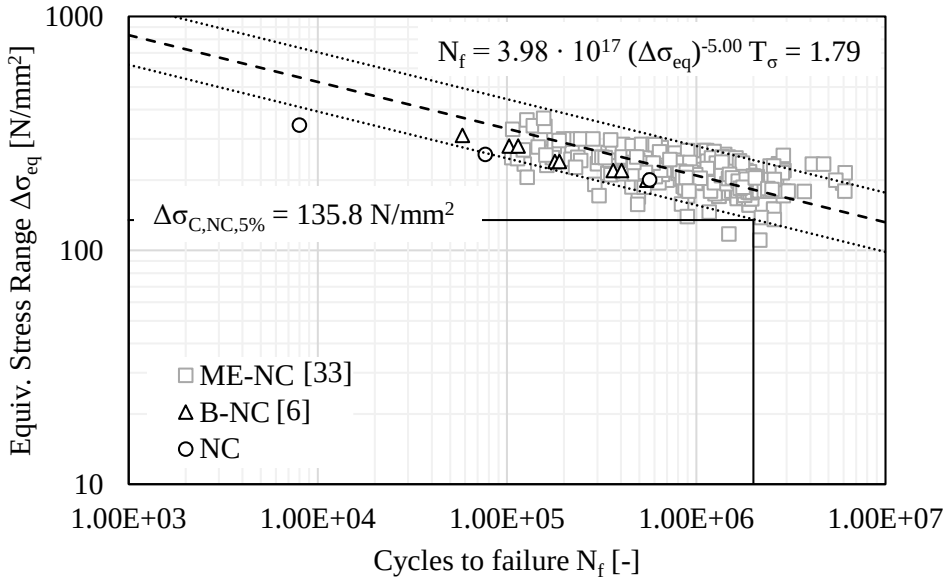

Figure 4 – Summary of experimental and literature results for uncoated specimens (NC: experimental tests; B-NC: Berto et al. [6]; ME-NC: Maljaars & Euler [33]).

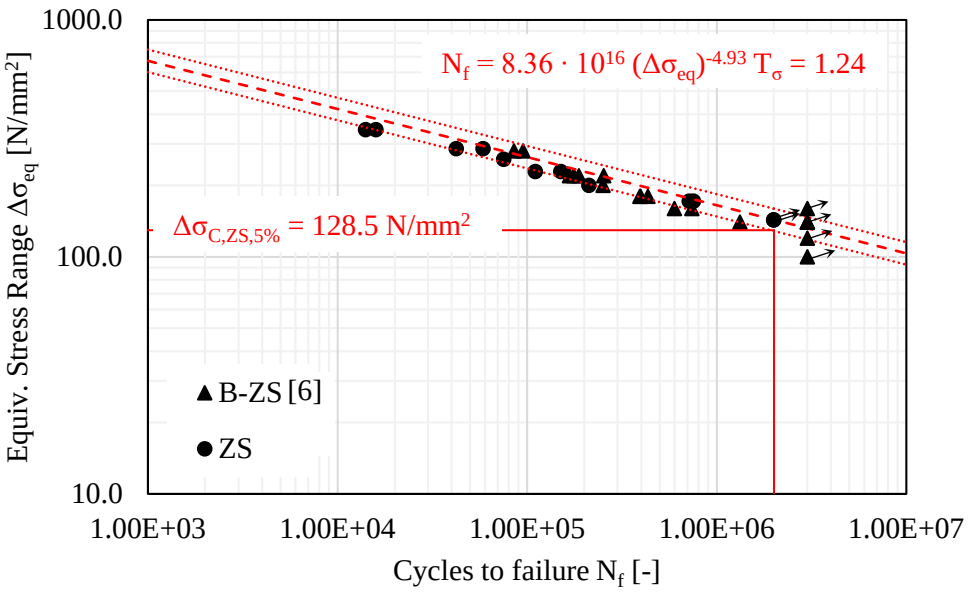

Figure 5 – Summary of experimental and literature results for coated & blasted specimens (ZS: experimental tests; B-ZS: Berto et al. [6]).

$$\Delta\sigma_{eq} = \Delta\sigma \cdot \frac{1 - \xi R}{1 - R} \tag{1}$$

with $\Delta\sigma_{eq}$ being the mean-stress corrected (equivalent) stress range and ξ being a mean-stress sensitivity factor depending on the structural detail of concern. According to Maljaars & Euler [33], $\xi = 0.4$ was assumed for investigated specimens.

Table 3 – Statistical assessment of experimental and literature results.

Specimens [-]	Source [-]	Upper DC $\Delta\sigma_{C,95}$ [N/mm²]	Mean DC $\Delta\sigma_{C,50}$ [N/mm²]	Characteristic DC $\Delta\sigma_{C,5}$ [N/mm²]	Inv. Slope m [-]	SR T_σ [-]
NC B-NC ME-NC	Section 2.2 Berto et al. [6] Maljaars & Euler [33]	243.5	181.9	135.8	5.00	1.79
ZS B-ZS	Section 2.2 Berto et al. [6]	160.0	143.4	128.5	4.93	1.24

As noticeable in Figure 4, experimental outcomes (see Section 2.2) and results from Berto et al. [6] for uncoated samples can be ascribed to the same scatter band identified by data reported in Maljaars & Euler [29], i.e., with the only exception of NC02 ($\Delta\sigma = \Delta\sigma_{eq} = 250$ N/mm², $N_f = 7996$), which slightly falls outside the 5% lower bound. This plausibly descends from non-negligible plasticity phenomena, as $\Delta\sigma > f_y$ for NC02. Remarkably, in spite of the multiple configurations considered (i.e., lap-shear and butt-joints, featuring 1 ÷ 11 bolts and 3 ÷ 5 plates having variable thickness – t = 8.5 ÷ 15 mm – and steel grade [6, 33, 42-49]), the scatter ratio for NC fatigue data is reasonably low ($T_{\sigma,NC} = 1.79$).

The resulting characteristic DC ($\Delta\sigma_{C,5,NC}$ = 135.8 N/mm^2, see Table 3) largely meets EN1993:1-9 [34] and DNVGL-RP-C203 [34] safety requirements (+21%).

As for coated & blasted specimens, statistical assessment of both ZS and B-ZS specimens results in a thinner, yet different scatter band as respect to uncoated samples ($T_{\sigma,ZS}$ = 1.24). On one hand, in compliance with literature remarks [6-20], the characteristic value of DC ($\Delta\sigma_{C,5,ZS}$ = 128.5 N/mm^2, see Table 3) is slightly lower than the corresponding value for uncoated joints (≈ –6%). On the other hand, a comparable inverse slope is derived for ZS/B-ZS Wöhler curves (m = 4.93, –2% as respect to NC samples).

Nevertheless, it is worth remarking that *i*) ZS curves still meet EN1993:1-9 [34] and DNVGL-RP-C203 [35] requirements in terms of characteristic fatigue strength (+15% as respect to the considered value, i.e. 112 N/mm^2, with the safety margin rising to +28% if DC 100 is assumed due to HDG [34]) and *ii*) derived slope is flatter as respect to normative indications (m = 3 for $N < N_D = 5 \cdot 10^6$ [34]/10^7 [35]).

In light of the above, it can be inferred that fatigue performance of double covered ZS high-strength bolted joints is moderately inferior as respect to pristine uncoated specimens. Hence, in the next Section, a corrosion-depending correction for Wöhler curves is introduced, i.e., in order to compare fatigue performance of coated samples as respect to corroded details based on indications reported in Adasooriya et al. [20-21] and DNVGL-RP-C203 [35].

2.4 Corrosion-affected Wöhler curves

According to indications reported in Adasooriya et al. [20-21], fatigue performance of corroded specimens can be inferred from pristine Wöhler curves by *i*) reducing the CAFL $\Delta\sigma_D$ up to a corrosion-affected value $\Delta\sigma_{D,corr.}$, *ii*) increasing the corresponding logarithmic slope $m_{corr.}$ and *iii*) assuming no fatigue limit for worn elements (that is, $m_{corr.} < \infty$ – Figure 6, green solid curve). It is worth remarking that the above method is intended to address corrosion fatigue from a global perspective. Namely, while applied stress ranges are still estimated on the reduced nominal cross-section (i.e., as in the ideal case of uniform corrosion), local sources of stress amplification due to non-uniform corrosion (“pitting”, which may strongly affect the fatigue performance of details [52-53]) are accounted for by penalizing S-N curves.

Based on analytical developments reported in Adasooriya et al. [20-21] and Milone et al. [2-3], $\Delta\sigma_{D,corr.}$ and $m_{corr.}$ (for $N_f \leq 5 \cdot 10^6$) can be estimated according to Equations (2-3):

$$\Delta\sigma_{D,corr.} = \Delta\sigma_D \cdot \left(\frac{\sigma_{\infty,corr.}}{\sigma_\infty}\right)^{0.9} = \Delta\sigma_D \cdot c^{0.9} \quad (2)$$

$$m_{corr.} = m \cdot \frac{3}{3 - m \log c} \quad (3)$$

with $c = \sigma_{\infty,corr.}/\sigma_\infty \leq 1$ being the endurance limit ratio among corroded and pristine details for $N_\infty = 10^7$ cycles. The entity of c – and hence the corresponding fatigue strength reduction – is derived from a statistical regression involving multiple specimens having the same (nominal) corrosion degree and yet different distributions of corrosion pits [20-21].

It is worth remarking that above expressions underlie the assumption that no reduction in fatigue strength is achieved for a threshold value of $N_{th} = 10^4$ cycles (that is, the effect of corrosion on low-cycle fatigue behaviour is supposed to be negligible [20-21]). Although similar expressions might be written for $N_f > 5 \cdot 10^6$, their analytical formulation is hence omitted, i.e., as the affected portion of fatigue domain is beyond the range of interest in terms of N_f values.

An alternative expedient is recommended in DNVGL-RP-C203 [35] for the fatigue assessment of unprotected details exposed to marine environment. For instance, pristine Wöhler curves for a given detail class are translated downward by replacing the S-axis intercept for $N_f = 1$ ($\log \bar{a}_1$) with a reduced value $\log \bar{a}_{1,corr.}$ depending on the relevant DC (Figure 6, green dash-dotted curve). Moreover, the adoption of a constant slope ($m = 3$) is recommended for curves related to corroded details.

Formulations reported in Adasooriya et al. [20-21] and DNVGL-RP-C203 [35] can be easily manipulated to derive the reference DC for a corroded detail $\Delta\sigma_{C,corr.}$ (Equations (4-5)), thus providing a synthetic indicator for fatigue performance comparisons (see next Sections for further details):

$$\text{Adasooriya et al.} \rightarrow \Delta\sigma_{C,corr.} = \Delta\sigma_C \cdot \left(\frac{5}{2}\right)^{-\frac{1}{3}\log c} \cdot c^{0.9} \quad (4)$$

$$\text{DNVGL-RP-C203} \rightarrow \Delta\sigma_{C,corr.} = \Delta\sigma_C \cdot \left(\frac{a_{1,corr.}}{a_1}\right)^{\frac{1}{3}} \quad (5)$$

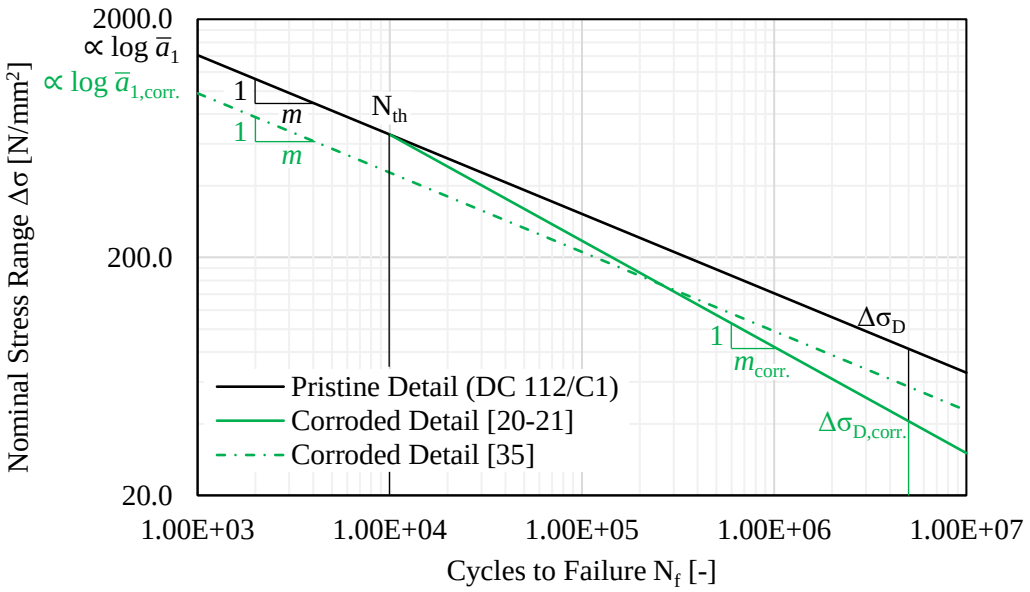

Figure 6 – Corrosion-depending corrections for Wöhler curves according to Adasooriya et al. [20-21] and DNVGL-RP-C203 [35].

3 Results and Discussion

3.1 Fatigue Performance of NC, ZS and Corroded High-Strength Bolted Details

Figure 7 depicts the comparison of fatigue performance of uncoated, coated & blasted and corroded high-strength bolted details in terms of relevant characteristic Wöhler curves (CI = 75%, P_F = 5%). For the sake of clarity, Wöhler curves related to all considered uncoated (NC + ME-NC + B-NC) and coated & blasted (ZS + B-ZS) specimens are hence referred as $\overline{\text{NC}}$ and $\overline{\text{ZS}}$, respectively.

In order to account for the detrimental effect of corrosion on unprotected specimens, three alternative strategies were assumed, namely: *i*) correction of the $\overline{\text{NC}}$ curve [33] by means of expressions proposed by Adasooriya et al. [20-21] (Figure 7, green dotted curve, $\Delta\sigma_{C,5}$ = 74.8 N/mm^2), *ii*) correction of normative curves (DC 112/C1 [30-31]) according to Adasooriya et al. [20-21] (Figure 7, green solid line, $\Delta\sigma_{C,5}$ = 61.7 N/mm^2), *iii*) introduction of the corrosion-affected curve for DC C1 according to DNVGL-RP-C203 [35] recommendations (Figure 7, green dash-dotted line, $\Delta\sigma_{C,5}$ = 77.8 N/mm^2).

According to Adasooriya et al. [20-21], a mean value of c = 0.460 was assumed for calculations (that is, $\Delta\sigma_{D,corr.}$ = 0.497 $\Delta\sigma_D$). To this end, it is worth remarking that, while a characteristic value for c = 0.270 ($\Delta\sigma_{D,corr.}$ = 0.308 $\Delta\sigma_D$) was also provided by Adasooriya et al., mean value of c was hence selected to accomplish the most unfavourable comparison for ZS specimens.

As for DNVGL-RP-C203 [35] recommendations, a reduced S-axis intercept $\log \bar{a}_{1,corr.}$ = 11.972 was assumed for corroded C1 detail class ($\log \bar{a}_1$ = 12.449), thus resulting in a reduced detail class $\Delta\sigma_{C,corr.}$ = 77.8 N/mm^2 (– 30% as respect to pristine conditions).

It is worth remarking that, as widely reported in scientific literature [6, 16, 33], size-effect may play a role in the fatigue performance of bolted specimens (that is, both for uncoated and coated & blasted joints [6, 16, 33]). Nevertheless, for the relevant case of pristine and corroded 112/C1 details, no thickness-related correction was assumed. Indeed, connected elements in NC, ZS and B-ZS [6] specimens are always thinner than the reference value t_{ref} = 25 mm reported in DNVGL-RP-C203 (that is, after which size-effect becomes non-negligible [35]). As for experimental tests recollected by Maljaars & Euler [33, 42-49], no correction was assumed as well, i.e. due to the thickness of connected elements being in the range t = 8.5 ÷ 15 mm. (notably, such values comply with typical geometrical features assumed for bridge joints design [36, 37, 54]).

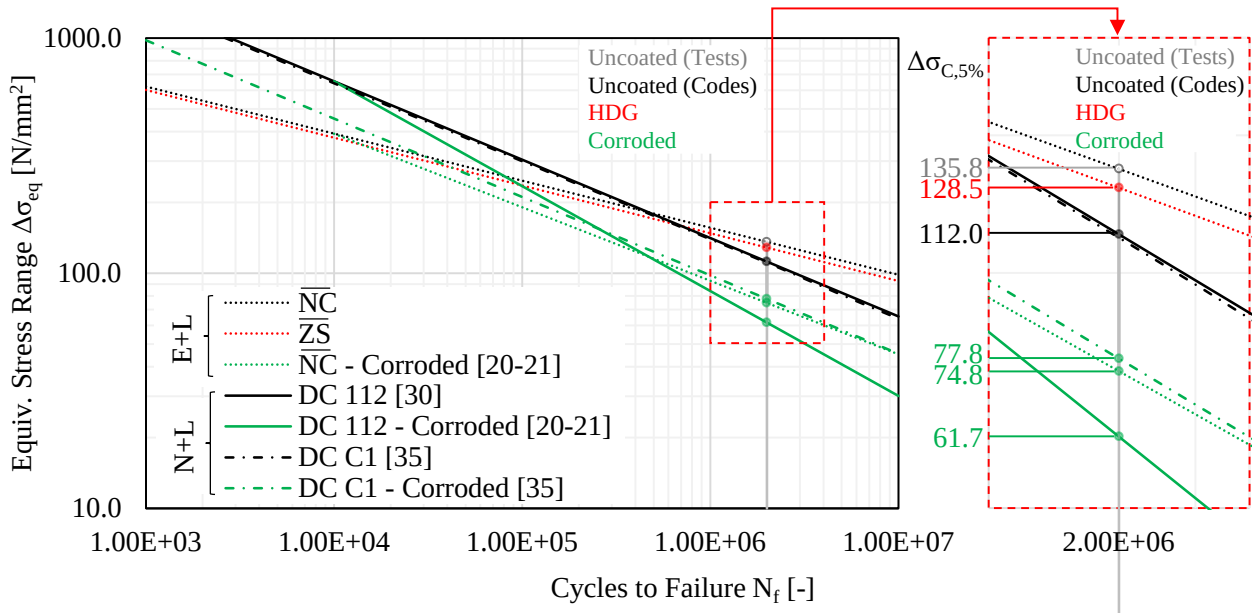

Figure 7 – Corrosion-depending corrections for Wöhler curves according to Adasooriya et al. [20-21] and DNVGL-RPC203 [35] (E+L: Experimental tests + Literature corrections; N+L: Normative provisions + Literature corrections; for the sake of simplicity, slope variation for $N_f \geq 5 \cdot 10^6$ is omitted).

Fatigue strength comparisons related to ZS, NC and corroded high-strength bolted details is summarized in Table 4 in terms of characteristic DCs $\Delta\sigma_{C,5}$ and inverse logarithmic slopes *m*.

Table 4 – Fatigue strength comparisons for ZS, NC and corroded specimens.

Specimens [-]	Characteristic DC $\Delta\sigma_{C,5}$ [N/mm²]	Inv. Slope *m* [-]*	Strength Variation Δ [%]**
NC	135.8	5.00	+5.7%
ZS	128.5	4.93	–
DC 112/C1 [34-35]	112.0	3.00	–12.9%
NC – Corroded [20-21]	74.8	3.20	–41.7%
DC 112 – Corroded [20-21, 34]	61.7	2.24	–52.0%
DC C1 – Corroded [35]	77.8	3.00	–39.5%
*Corrected slope according to Adasooriya et al. [20-21] being related to the range $10^4 \leq N_f \leq 5 \cdot 10^6$ **Strength variations being estimated assuming $\Delta\sigma_{C,5,ZS}$ as a reference value			

One can immediately observe that, although being only slightly inferior to uncoated pristine specimens, fatigue performance of ZS bolted joints is always higher as respect to corroded details, with a minimum gap Δ = 12.9% in terms of $\Delta\sigma_{C,5}$ when correcting the Wöhler curve for uncoated specimens with Adasooriya et al. [20-21] formulations. Such gap increases up to 63.1% if the characteristic value of c = 0.290 is assumed for calculations.

Interestingly, while $\overline{ZS}$ and $\overline{NC}$ curves are almost parallel to each other, the corrected $\overline{NC}$ curve is significantly steeper (m = 5.00, 4.93 and 3.20, respectively, see Table 4); hence, fatigue performance of ZS specimens can be deemed as superior as respect to corroded samples within the entire range of applicable stress ranges. While the slope of other corrected curves significantly differs from the $\overline{ZS}$ regression line (m = 2.24 ÷ 3.20), fatigue strength of coated & blasted bolted joints still exceeds the resistance of corroded details in high-cycle fatigue (HCF) conditions ($\approx N_f > 10^5$, see Figure 7), i.e., the most relevant regime for practical civil engineering purposes [2, 41, 54].

In light of the above, HDG can be deemed as a suitable solution for safeguarding high-strength bolted steel structures subjected to cyclic loads in an aggressive environment – that is, if significant corrosion fatigue damage would be expected in absence of protective measures – i.e., due to fatigue strength being more sensitive to the detrimental effect of corrosion as respect to galvanization treatment. Nevertheless, hot-dip zinc coating still reduces the fatigue performance of pristine double covered joints up to a moderate extent. To this end, the selection of an inferior DC for galvanized joints [34, 41] can be considered an appropriate design choice, although considered ZS specimens still meet normative requirements [34-35] for DC 112 with a relatively small margin of safety (+12.9%, see Table 4).

Interestingly, ZS pre-loaded bolted samples show a comparable strength decrease as respect to smooth specimens [13, 16, 29], i.e., in opposition to coated welded details such as cruciform joints – for which a negligible DC reduction was observed [13, 55].

In the first instance, this outcome can be related to the combined influence of galvanization and stress raising sources (e.g., bolt holes) [6, 32-33], with the latter being absent in plain components and welded details being already governed by *i*) stress singularity at weld toe and *ii*) material degradation within the heat-affected zone (HAZ) [55, 56]. Nevertheless, in order to provide a more in-depth investigation about the effect of HDG on high-strength bolted specimens, fracture surface analyses on ZS samples have been carried out. Further details are reported in the next Section.

3.2 Fracture Surfaces Analyses

Fracture surfaces for each specimen were investigated through scanning electron microscopy (SEM) technology. For this purpose, a Quanta 650 FEG SEM (Thermo Fisher Inc.) was operated at 20 kV accelerating voltage with a 30 µm aperture and a spot size of 3.0. A working distance of ≈30 mm was adopted in order to

get secondary electron images from the fracture surface. A peculiar attention was paid to detecting possible traces of hydrogen embrittlement (HE), which has been deemed to play a role in fracture of galvanized details by several researchers [57-65]. Figure 8 shows the crack initiation sites as derived from the fractographic investigations of specimens.

In case of ZS joints, the main crack always nucleates at the interface between the Zn layer and the steel core, i.e., both in case of moderate loads (ZS03, ΔF =140 kN, $\Delta\sigma$ =145.8 N/mm^2, see Figure 8a) and high loads (ZS06, ΔF = 240 kN, $\Delta\sigma$ = 250.0 N/mm^2, see Figure 8b). As for NC specimens, main cracks initiate on the L profiles' surface, that is, nearby the innermost bolt holes (see Figure 8c-d, specimens NC03 and NC02, $\Delta\sigma$ = 145.8 N/mm^2 and 250.0 N/mm^2, respectively). This outcome plausibly descends from the combined action of profile-gasket friction (i.e., the predominant mechanism for transferring shear actions in preloaded bolted connections [30, 33, 54]) and local stress amplifications at bolt holes. Moreover, a further amplification source for the observed crack spots is possibly represented by intrinsic imperfections and assembling tolerances that might lead to unaccounted secondary (out-of-plane) bending stresses.

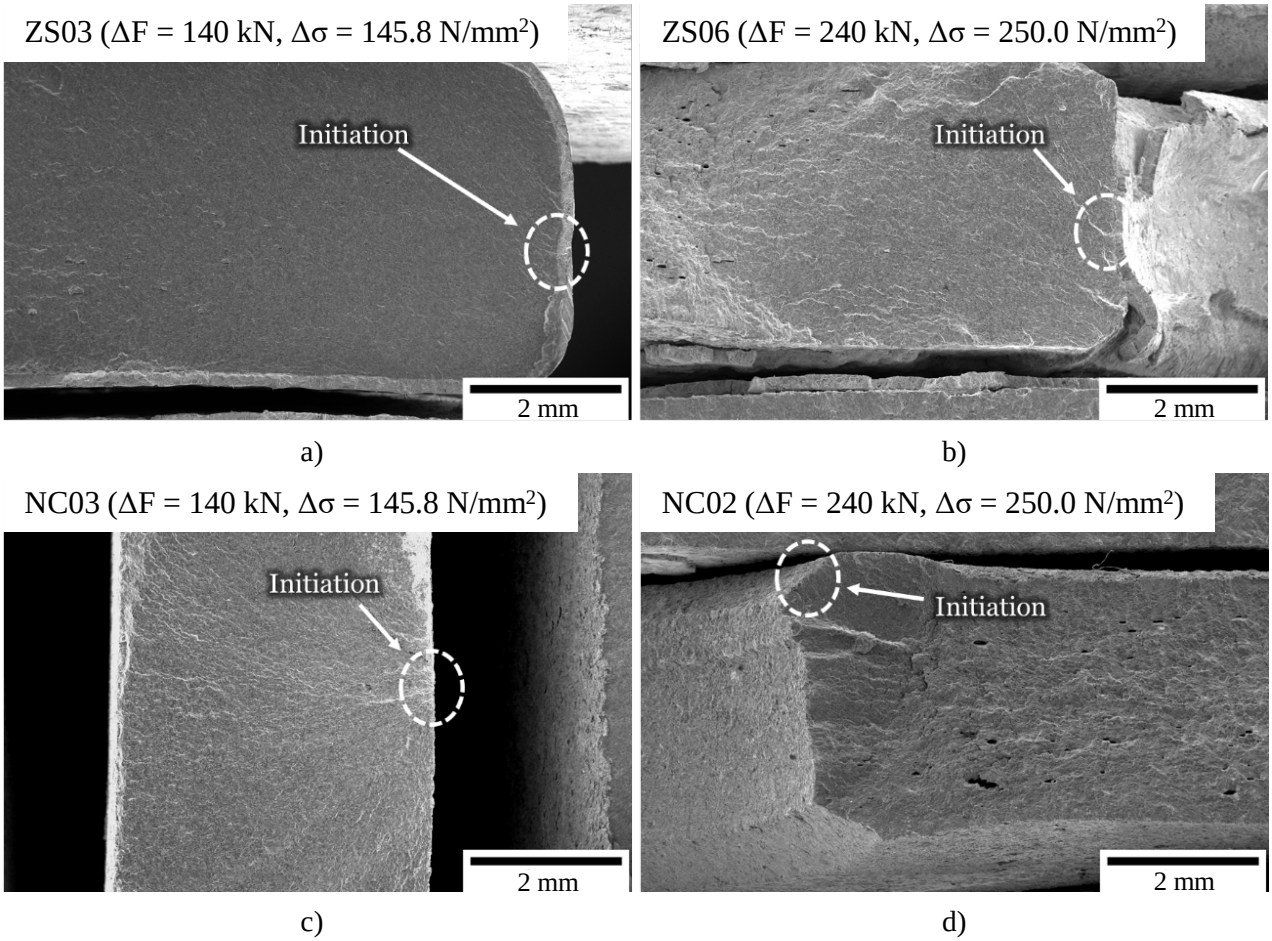

Figure 8 – Fractographies showing typical initiation sites in ZS (a-b) and NC (c-d) specimens under moderate and high stress ranges.

Further hints about crack initiation and propagation can be inferred by magnifying fractographic images, as depicted in Figure 9. For ZS specimens, crack initiation appears to be accompanied with some brittle-like features such as intergranular (IG) fracture, while the main crack grows in a transgranular (TG) manner (see Figure 9a, specimen ZS02). Nevertheless, when the applied stress range is increased (see Figure 9b, specimen ZS06), brittle features are absent and only TG-type striations can be seen on the fracture surface. Contrariwise, in case of NC joints only TG-type striations can be observed, i.e., independently of the actual value of $\Delta\sigma$. Interestingly, a common feature among both coated and uncoated specimens is represented by the potential trigger of secondary cracks. Namely, they can be observed for elevated loads in both cases (Figure 9b-d), while they are uncommon for lower $\Delta\sigma$ values (Figure 9a-c).

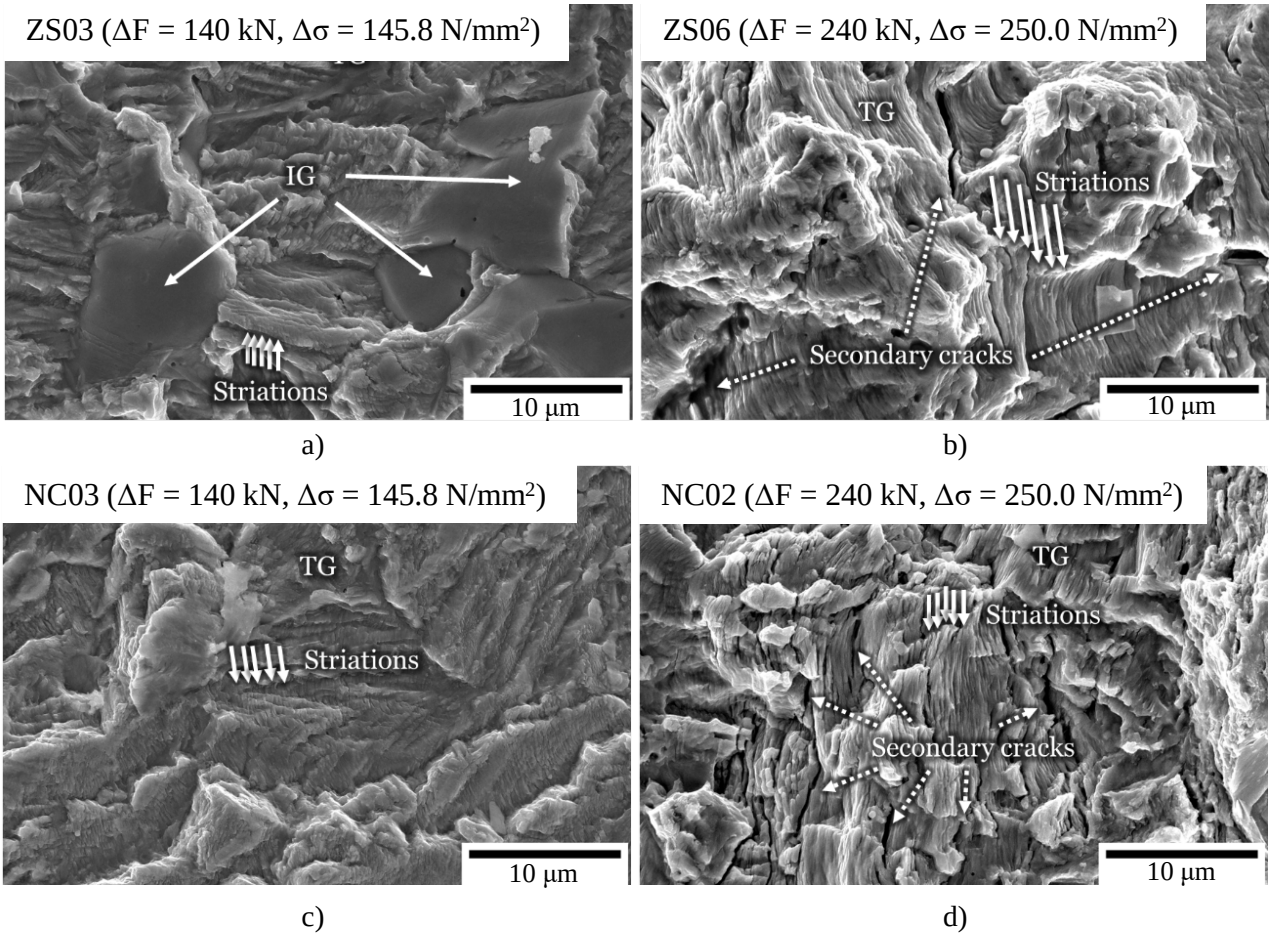

Figure 9 – Fracture features nearby initiation sites shown in Figure 8: a) ZS03, b) ZS06, c) NC03, d) NC02.

For thoroughness, detailed fractographic investigations for ZS specimens under other loading levels are reported in Figure 10, i.e. providing a coverage of all considered stress ranges within the present study.

Interestingly, it can be observed that, while the main crack grows in a TG manner, some brittle features such as IG and quasi-cleavage (QC) fracture can be always appreciated up to a threshold value of $\Delta\sigma \leq 208.3$ N/mm^2

($\Delta F \leq 200$ kN, see Figure 10a-b-c-d). Contrariwise, as stated above, specimen tested at the highest load level ($\Delta F = 240$ kN, $\Delta\sigma = 250$ N/mm^2, see Figure 9b) does not show significant brittle features. The opposite trend is shown by secondary cracks, the occurrence of which becomes more and more common for increasing loads up to the highest considered stress range.

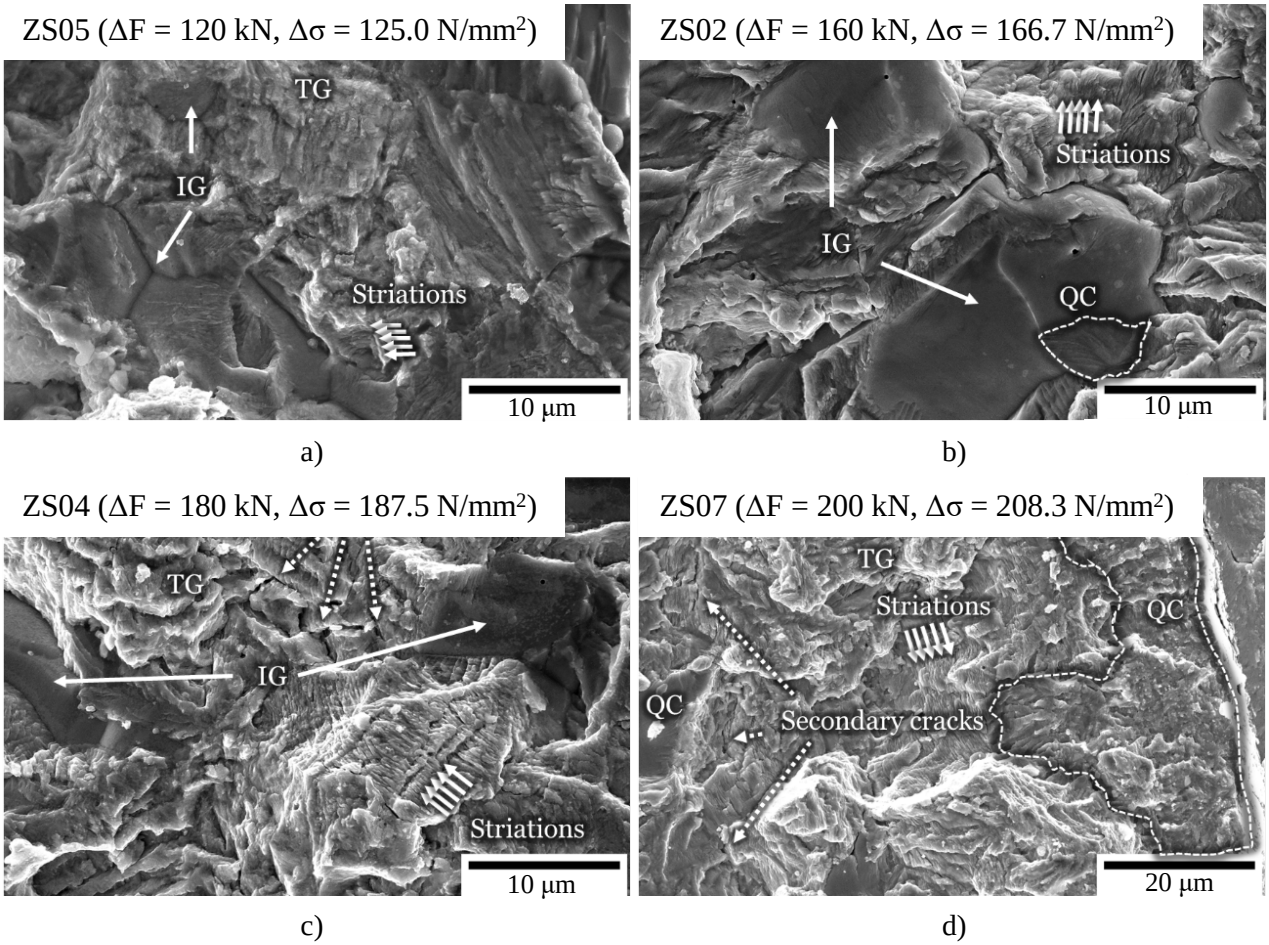

Figure 10 – Fracture features nearby initiation sites for ZS specimens under different load levels: a) ZS05, b) ZS02, c) ZS04, d) ZS07.

The above outcomes from reported fractographic investigations suggest that HE could actually influence the fatigue failure of coated & blasted specimens. Namely, while the crack initiation generally occurs in stress-concentrated sites on the surface of NC samples, in case of ZS specimens the cracks initiate at the interface between the Zn layer and the base-steel.

To this end, it is worth reporting that Jeon et al. [57] suggested that Zn coating can act as a barrier for hydrogen permeation, i.e., due to the formation of a Zn passive film at the surface which reduces the hydrogen evolution rate. Nevertheless, the same Zn layer may also hinder the out-diffusion of internal hydrogen which could have

been introduced during previous processes (e.g., during hot-dip galvanization), thus resulting in an embrittlement effect [58].

As a matter of fact, typical evidences of hydrogen-assisted fatigue crack growth can be identified as IG- and QC-type fracture features, e.g., as observed in pure Fe [59-60], Fe-3wt%Si [61-62], medium-Mn steels [63] and X70 pipeline steels [64]. Such features are quite similar to the ones observed in tested galvanized samples shown in Figures 9-10.

Although further studies are needed, it has also been suggested that HE may further intensify when a galvanized component is in contact with an alkaline environment, e.g., in a water-containing environment which is suitable for water hydrolysis. Indeed, in this case the hydrogen evolution can directly take place on the galvanized surface, thus resulting in an even higher level of brittleness [65].

Nevertheless, it is worth remarking that the brittle-like features disappear for the highest load levels. This outcome plausibly descends from fatigue crack growth being dominated by load-controlled mechanisms for elevated stress ranges, with the hydrogen-metal interaction becoming less influent. This complies with the increasing formation rate of secondary cracks for higher $\Delta\sigma$ values, which proved to be insensitive to the presence of a Zn coating (Figure 9).

4 Conclusions

In the present work, the influence of hot-dip galvanization on the fatigue performance of high-strength bolted specimens was thoroughly investigated. To this end, a set of 15 constant-amplitude fatigue tests was carried out. Fatigue data were hence statistically assessed and compared against *i*) results for uncoated, pristine specimens drawn from literature [6, 33] and *ii*) literature and normative indications for unprotected details in an aggressive environment [20-21, 35]. Subsequently, fracture surfaces of galvanized specimens were investigated through SEM technology. In light of the achieved results, the following conclusive remarks can be pointed out:

- The characteristic fatigue strength $\Delta\sigma_{C,5}$ of the investigated high-strength bolted details is 135.8 N/mm^2 at $2 \cdot 10^6$ cycles (higher than the DC 112/C1 suggested in standards [34-35]) in pristine conditions while for the investigated coated & blasted specimens is 128.5 N/mm^2 at $2 \cdot 10^6$ cycles resulting in a reduction of ≈6% due to the galvanization;
- Nevertheless, the process of hot-dip galvanization can results in a fatigue resistance $\Delta\sigma_{C,5,ZS}$ of [*1.13*; *1.52*] times higher as respect to unprotected joints exposed to aggressive environment (according to literature models to evaluate the detrimental effects of corrosion [20-21, 35]);
- ZS high-strength bolted specimens appear to be more influenced by the coating process as respect to welded details [13, 16, 55]. This descends from the combined effect of galvanization and light notch effect at bolt holes;
- Fracture surfaces of failed ZS specimens were investigated through SEM inspection. Accordingly, hydrogen embrittlement may play an important role as respect to the fatigue performance of galvanized specimens, as the Zn layer hinders the out-diffusion of hydrogen embodied during the molten bath;
- Nevertheless, the influence of HDG appears to be less pronounced for higher load levels, as load-controlled mechanisms become more and more predominant, as testified by the increasing occurrence of secondary cracks.

References

[1] Milone A, Landolfo R, Berto F. Methodologies for the fatigue assessment of corroded wire ropes: A state-of-the-art review. *Structures* 2022, 37, 787-794.

[2] Milone A, Landolfo R. A Simplified Approach for the Corrosion Fatigue Assessment of Steel Structures in Aggressive Environments. *Materials* 2022, 15(6), 2210.

[3] El-Reedy MA. Corrosion Protection – Chapter 6 of Offshore Structures – 2nd Edition. Gulf Professional Publishing 2020, Oxford, UK, 359-417.

[4] Farh HMH, Ben Seghier MEA, Zayed T. A Comprehensive Review of Corrosion Protection and Control Techniques for Metallic Pipelines. *Engineering Failure Analysis* 2023, 143, 106885.

[5] Jiang JH, Ma AB, Weng WF, Fu GH, Zhang YF, Liu GG, Lu FM. Corrosion Fatigue Performance of Presplit Steel Wires for High Strength Bridge Cables, *Fatigue & Fracture of Engineering Materials & Structures* 2009, 32, 769-779.

[6] Berto F, Mutignani F, Guido E. Effect of Hot Dip Galvanization on the Fatigue Behaviour of Steel Bolted Connections. *International Journal of Fatigue* 2016, 93, 168-172.

[7] Yang WJ, Yang P, Li XM, Feng WL. Influence of Tensile Stress on Corrosion Behaviour of High Strength Galvanized Steel Bridge Wires in Simulated Acid Rain, *Materials and Corrosion* 2012, 63, 401-407.

[8] Berchem K, Hocking MG. The Influence of Pre-Straining on the Corrosion Fatigue Performance of Two Hot-Dip Galvanised Steels, *Corrosion Science* 2006, 48, 4094-4112.

[9] Berchem K, Hocking MG. The Influence of Pre-Straining on the High-cycle Fatigue Performance of Two Hot-dip Galvanised Car Body Steels, *Materials Characterization* 2006, 58, 593-602.

[10] James MN. Designing against LMAC in Galvanised Steel Structures, *Engineering Failure Analysis* 2009, 16, 1051-1061.

[11] Di Cocco V. Sn and Ti Influences on Intermetallic Phases Damage in Hot Dip Galvanizing. *Frattura ed Integrità Strutturale* 2012, 22, 31-38.

[12] Kuklik V, Kudlacek J. Hot-Dip Galvanizing of Steel Structures. Butterworth-Heinemann 2016. Oxford, UK.

[13] Ferraz G, Rossi B. On the Fatigue Behaviour of Hot Dip Galvanized Structural Steel Details. *Engineering Failure Analysis* 2020, 118, 104834.

[14] Berto F, Mutignani F, Tisalvi M. Notch Effect on the Fatigue Behavior of a Hot Dip Galvanized Structural Steel. *Strength of Materials* 2015, 719-727.

[15] Rademacher D. Zur sicheren Anwendung feuerverzinkter Bauteile im Stahl- und Verbundbrückenbau, TU Dortmund 2017 [PhD Thesis, In German].

[16] Ungermann D, Rademacher D, Oechsner M, Simonsen F, Friedrich S, Lebelt P. Design of Hot-Dip Galvanized Bridges. Procedia of the 7th European Conference on Steel and Composite Structures (EUROSTEEL) 2014. Naples, Italy.

[17] Bergengren Y, Melander A. An experimental and Theoretical Study of the Fatigue Properties of Hot Dip-galvanized High Strength Sheet Steel. *International Journal of Fatigue* 1992, 14, 154-162.

[18] Nilsson T, Engberg G, Trogen H. Fatigue Properties of Hot-dip Galvanized Steels. *Scandinavian Journal of Metallurgy* 1989, 18, 166-175.

[19] Browne RS, Gregory EN, Harper S. The Effects of Galvanizing on the Fatigue Strengths of Steels and Welded Joints. *Procedia of the Seminar on Galvanizing of Silicon Containing Steels* 1975, ILZRO Publishers, Liege, 246-264.

[20] Vogt JB, Boussac O, Foct J. Prediction of Fatigue Resistance of a Hot-dip Galvanized Steel. *Fatigue & Fracture of Engineering Materials & Structures* 2000, 23, 33-39.

[21] Adasooriya ND, Hemmingsen T, Pavlou D. Fatigue Strength Degradation of Metals in Corrosive Environments. *IOP Conference Series: Materials Science and Engineering* 2017, 276, 012039.

[22] Adasooriya ND, Pavlou D, Hemmingsen T. Fatigue Strength Degradation of Corroded Structural Details: A formula for S-N curve. *Fatigue & Fracture of Engineering Materials & Structures* 2020, 43, 721-733.

[23] Jiang C, Wu C, Jiang X. Experimental Study on Fatigue Performance of Corroded High-strength Steel Wires Used in Bridges. *Construction and Building Materials* 2018, 187, 681-690.

[24] Jikal FM, Chaffou H, Meziane M, El Ghorba M. Corrosion Influence on Lifetime Prediction to Determine the Wohler Curves of Outer Layer Strand of a Steel Wire Rope. *Engineering Failure Analysis* 2020, 109, 104253.

[25] Zampieri P, Curtarello A, Maiorana E, Pellegrino C. Fatigue Strength of Corroded Bolted Connection. *Frattura ed Integrità Strutturale* 2018, 43, 90-95.

[26] Lachowicz MB, Lachowicz MM. Influence of Corrosion on Fatigue of the Fastening Bolts. *Materials* 2021, 14, 1485.

[27] Li L, Li Y, Shi W, Li CQ. Deterioration of Fatigue Strength of Bolted Connection Plates Under Combined Corrosion and Fatigue. *Journal of Constructional Steel Research* 2021, 179, 106559.

[28] Jiang C, Xiong W, Cai CS, Zhou X, Zhu Y Corrosion Effects on the Fatigue Performance of High-Strength Bolted Friction Connections. *International Journal of Fatigue* 2023, 168,107392.

[29] Ungermann D, Rademacher D, Oechsner M, Landgrebe R, Adelmann J, Simonsen F, Friedrich S, Lebelt P. P 835 - Feuerverzinken im Stahl- und Verbundbrückenbau. FOSTA e.V. 2014. Dusseldorf, Germany [In German].

[30] Tartaglia R, D'Aniello M, Zimbru M. Experimental and Numerical Study on the T-Stub Behaviour with Preloaded Bolts under Large Deformations. *Structures* 2020, 27, 2137-2155.

[31] RFI (Italian Railway Network). RFI DTC INC PO SP IFS 003 A: Specifica per la Verifica a Fatica dei Ponti Ferroviari. RFI 2011. Rome, Italy [In Italian].

[32] Landolfo R, Cascini L, D'Aniello M, Portioli F. Gli effetti del degrado da fatica e corrosione sui ponti ferroviari in carpenteria metallica: Un approccio integrato per la valutazione della vita residua. *Costruzioni Metalliche* 2010, 6, 37-46 [In Italian].

[33] Maljaars J, Euler M. Fatigue S-N curves of Bolts and Bolted Connections for Application in Civil Engineering Structures. *International Journal of Fatigue* 2021, 151, 106355.

[34] CEN (European Committee for Standardization). EN1993:1-9 – Eurocode 3: Design of Steel Structures, Part 1-9: Fatigue. CEN 2005. Brussel, Belgium.

[35] DNV (Det Norske Veritas). DNVGL-RP-C203 - Fatigue Design of Offshore Steel Structures. DNV 2016. Bærum, Norway.

[36] Unsworth JF. Design and Construction of Modern Steel Railway Bridges – 2nd Edition. CRC Press 2017. Boca Raton, FL, USA.

[37] Denton S. Bridge Design to Eurocodes: UK Implementation – 1st Edition. ICE Publications 2011. London, UK.

[38] CEN (European Committee for Standardization). EN1993:1-8 – Eurocode 3: Design of Steel Structures, Part 1-8: Design of Joints. CEN 2005. Brussel, Belgium.

[39] ISO (International Organization for Standardization). ISO 10684 – Fasteners – Hot dip galvanized coatings. ISO 2004. Geneva, Switzerland.

[40] ISO (International Organization for Standardization). ISO 8503 – Preparation of steel substrates before application of paints and related products. ISO 2012. Geneva, Switzerland.

[41] Schijve J. Fatigue of Structures and Materials. Springer-Verlag 2009. Berlin, Germany.

[42] Albrecht P, Sahli AH, Wattar F. Fatigue Strength of Bolted Joints. *Journal of Structural Engineering* 1987, 113(8), 1834-1849.

[43] Brown JD. Punched Holes in Structural Connections, University of Texas 2006 [PhD Thesis].

[44] Frank KH, Yura JA. An Experimental Study of Bolted Shear Connections, University of Texas 1981 [Technical Report].

[45] Kulak GL, Fisher JW, Struik JHA. Guide to Design Criteria for Bolted and Riveted Joints. ASCE Press 2001, Chicago, IL, USA.

[46] Lieurade HP. Étude de la Tenue a la Fatigue des Assemblages Boulonnés en Aciers a Haute Limite d'Élasticité. *Construction Métallique* 1977, 1, 59-65 [In French].

[47] Mas E, Janss J. Assemblages par boulons a haute resistance. Fatigue des assemblages a double couvre-joint. CRIF 1964 [In French].

[48] OTO (Offshore Technology Organization). OTO 97067 – Offshore Technology Report – Fatigue Tests on Steel Bolts. OTO 1997.

[49] Valtinat G, Huhn H. Bolted Connections with Hot Dip Galvanized Steel Members with Punched Holes. *Connections in Steel Structures* 2004, 5, 297-310.

[50] CEN (European Committee for Standardization). prEN1993:1-9-2020 – Eurocode 3: Design of Steel Structures, Part 1-9: Fatigue – 2020 Draft. CEN 2020. Brussel, Belgium [Draft].

[51] Dowling NE, Calhoun CA, Arcari A. Mean Stress Effects in Stress-Life Fatigue and the Walker Equation. *Fatigue & Francture of Engineering Materials & Structures* 2009, 32(3), 163-179.

[52] Shojai S, Schaumann P, Braun M, Ehlers S. Influence of Pitting Corrosion on the Fatigue Strength of Offshore Steel Structures Based on 3D Surface Scans. *International Journal of Fatigue* 2022, 164, 107128.

[53] Shamir M, Braithwaite J, Mehmanparast A. Fatigue Life Assessment of Offshore Wind Support Structures in the Presence of Corrosion Pits. *Marine Structures* 2023, 92, 103505.

[54] ECCS (European Convention for Constructional Steelwork). Fatigue Design of Steel and Composite Structures – 2nd Edition. Ernst & Sohn 2018. Berlin, Germany.

[55] Berto F, Fergani O. Fatigue Behaviour of Welded Structural Steel Subjected to Hot-dip Galvanization Process. *International Journal of Fatigue* 2017, 101(2), 439-447.

[56] Berto F, Lazzarin P. Recent Developments in Brittle and Quasi-Brittle Failure Assessment of Engineering Materials by Means of Local Approaches. *Materials Science and Engineering R: Reports* 2014, 75(1), 1-48.

[57] Jeon HH, Lee SM, Han J, Park IJ, Lee YK. The Effect of Zn Coating Layers on the Hydrogen Embrittlement of Hot-Dip Galvanized Twinning-Induced Plasticity Steel. *Corrosion Science* 2016, 111, 267-274.

[58] Jo KR, Cho L, Sulistiyo DH, Seo EJ, Kim SW, De Cooman BC. Effects of Al-Si Coating and Zn Coating on the Hydrogen Uptake and Embrittlement of Ultra-High Strength Press-Hardened Steel. *Surface and Coatings Technology* 2019. 374, 1108-1119.

[59] Ogawa Y, Birenis D, Matsunaga H, Takakuwa O, Yamabe J, Prytz O, Thogersen A. The Role of Intergranular Fracture on Hydrogen-Assisted Fatigue Crack Propagation in Pure Iron at a Low Stress Intensity Range. *Materials Science and Engineering: A* 2018, 733,316-328.

[60] Shinko T, Hénaff G, Halm D, Benoit G, Bilotta G, Arzaghi M. Hydrogen-Affected Fatigue Crack Propagation at Various Loading Frequencies and Gaseous Hydrogen Pressures in Commercially Pure Iron. *International Journal of Fatigue* 2019, 121, 197-207.

[61] Wan D, Deng Y, Meling JIH, Alvaro A, Barnoush A. Hydrogen-Enhanced Fatigue Crack Growth in a Single-Edge Notched Tensile Specimen under In-Situ Hydrogen Charging Inside an Environmental Scanning Electron Microscope. *Acta Materialia* 2019, 170, 87-99.

[62] Wan D, Alvaro A, Olden V, Barnoush A. Hydrogen-Enhanced Fatigue Crack Growth Behaviors in a Ferritic Fe-3wt%Si Steel Studied by Fractography and Dislocation Structure Analysis. *International Journal of Hydrogen Energy* 2019, 44(10), 5030-5042.

[63] Wan D, Ma Y, Sun B, Razavi SMJ, Wang D, Lu X, Son W. Evaluation of Hydrogen Effect on The Fatigue Crack Growth Behavior of Medium-Mn Steels via In-Situ Hydrogen Plasma Charging in an Environmental Scanning Electron Microscope. *Journal of Materials Science & Technology* 2021, 85, 30-43.

[64] Alvaro A, Wan D, Olden V, Barnoush A. Hydrogen Enhanced Fatigue Crack Growth Rates in a Ferritic Fe-3 Wt%Si Alloy and a X70 Pipeline Steel. *Engineering Fracture Mechanics* 2019, 219, 106641.

[65] Recio FJ, Alonso MC, Gaillet L, Sanchez M. Hydrogen Embrittlement Risk of High Strength Galvanized Steel in Contact with Alkaline Media. *Corrosion Science* 2011, 53(9), 2853-2860.